Applied Catalysis B: Environmental 147 (2014) 29–34

Contents lists available at ScienceDirect

Applied Catalysis B: Environmental

journal homepage: www.elsevier.com/locate/apcatb

Long-lived photogenerated charge carriers of 0 0 1-facet-exposed TiO_2 with enhanced thermal stability as an efficient photocatalyst

Yunbo Luan [a,b], Liqiang Jing [a,*], Jing Wu [a], Mingzheng Xie [a,b], Yujie Feng [b,**]

[a] Key Laboratory of Functional Inorganic Materials Chemistry (Heilongjiang University), Ministry of Education, School of Chemistry and Materials Science, Harbin 150080, PR China
[b] State Key Lab of Urban Water Resource and Environment (Harbin Institute of Technology), Harbin 150001, PR China

ARTICLE INFO

Article history:
Received 1 June 2013
Received in revised form 12 August 2013
Accepted 15 August 2013
Available online 26 August 2013

Keywords:
Exposed 0 0 1 facet
Thermal stability
Long-lived carrier
Charge separation
Photocatalysis

ABSTRACT

The thermal stability of the (0 0 1) facet-exposed nanocrystalline TiO_2 with high photocatalytic activity is often neglected although it is generally needed to be subjected to certain high-temperature treatment for applications. Herein, it is found that the (0 0 1) facet exposure percentage of nanocrystalline anatase TiO_2 could be decreased from 71% to 25% when the thermal treatment temperature is raised from 100 to 500 °C. Interestingly, its thermal stability is greatly enhanced after phosphate modification, even slightly changed for the 0 0 1-facet-exposed percentage (67%) after thermal treatment at 650 °C. It is suggested for the first time that the enhanced thermal stability mainly depends on the modified phosphate groups with high thermal stability binding strongly to the exposed 0 0 1 facet of TiO_2. More important, it is confirmed that the enhanced thermal stability greatly prolongs lifetime and promotes separation of photogenerated charge carriers of 0 0 1-facet-exposed TiO_2 mainly by means of time-resolved surface photovoltage responses, leading to the obviously improved photocatalytic activity for degrading liquid-phase phenol and gas-phase acetaldehyde. This is attributed to the synergetic effects of high-percentage 0 0 1-facet exposure, high anatase crystallinity, and strong ability to adsorb O_2.

1. Introduction

Anatase TiO_2 has been widely investigated due to its promising applications in photocatalysis, photovoltaic cells, sensors, and for photosplitting water. Recently, theoretical and experimental studies have demonstrated that, the (0 0 1) facets of anatase TiO_2 are much more reactive than the thermodynamically more stable (1 0 1) surface due to higher average surface energy of the (0 0 1) facets than that of the (1 0 1) facets [1,2]. Unfortunately, surfaces with high reactivity usually diminish rapidly during the crystal growth process as a result of the minimization of surface energy. Most available anatase TiO_2 crystals are dominated by the thermodynamically stable (1 0 1) facets, rather than the much more reactive (0 0 1) facets. Until Yang et al. discovered that introducing HF could reverse the relative stability of (0 0 1) and (1 0 1) faces in 2008, a pioneering breakthrough in the synthesis of anatase TiO_2 with exposed (0 0 1) facet was accomplished [3]. Following the breakthrough, other researchers further confirm that the presence of fluorine species plays an important role in the formation of 0 0 1-facet exposed TiO_2 and finally could remain on the surface of TiO_2 [4,5]. Interestingly, it is clearly demonstrated that the high-energy 0 0 1 facet, along with the surface residual fluoride, is much favorable for efficient photocatalytic reactions on TiO_2 [6,7].

To expand its application, like as films and coatings, it is often required for the 0 0 1-facet exposed TiO_2 obtained to be subjected to the high temperature thermal treatment. It is widely accepted that fluorine species play a vital role in keeping the stability of (0 0 1) facets during the growing process of TiO_2 crystallite. However, the residual fluoride species on the surfaces of the resulting TiO_2 is not thermally stable so that it is easily left away after thermal treatment at high temperature of over 450 °C, based on our previous work and other reports [8,9]. Thus, we naturally come to predict that the disappearance of surface residual fluoride would influence the thermal stability of high-energy 0 0 1 facet so as to greatly decrease its photocatalytic performance. To the best of our knowledge, the thermal stability of exposed 0 0 1 facet of nanocrystalline anatase TiO_2 is often ignored. Different from hydrofluoric acid, phosphoric acid is thermally stable so that it could be firmly fixed on the surfaces of TiO_2 after thermal treatment at the high temperature of 800 °C [10]. Worthy of speaking, the phosphate modification could promote the O_2 adsorption so as to improve the photogenerated charge separation of TiO_2 [11]. Based on the above consideration, we try to modify the synthesized high-percentage 0 0 1-facet exposed nanocrystalline TiO_2 with phosphoric acid, aiming to overcome the expected issues so as to keep high or even much

* Corresponding author. Tel.: +86 451 86608616; fax: +86 451 86673647.
** Corresponding author.
E-mail address: Jinglq@hlju.edu.cn (L. Jing).

0926-3373/$ – see front matter © 2013 Elsevier B.V. All rights reserved.
http://dx.doi.org/10.1016/j.apcatb.2013.08.029

high photocatalytic activity after thermal treatment at high temperature. It is of great significance for environmental photocatalysis from engineering and scientific points.

2. Experimental

All substances used in this study are analytical grade and used without further purification. Deionized water is used in all experiments.

2.1. Synthesis of materials

Nano-sized TiO_2 with high-percentage (0 0 1)-facet exposure is prepared by HF-modified hydrothermal method as follows. In a typical procedure, 5 mL of $Ti(OBu)_4$ is mixed with 20 mL of absolute ethanol under vigorously stirring. After that, hydrofluoric acid solution (0.9 mL, 40%) is added. The resulting solution is stirred for 1 h, transferred in a Teflon lined stainless-steel autoclave, and then kept at 160 °C for 24 h. After being cooled to room temperature, the white precipitate is collected, washed with ethanol and water for several times in turn. To complete the modification, the white precipitate is put into 30 mL of different concentration of phosphoric acid solution. Then, the resulting suspension is stirred for 4 h, centrifuged, and washed with water two times. Finally, the TiO_2 modified with different amounts of phosphoric acid is obtained by drying and calcining at different temperature for 2 h. The obtained unmodified powder is denoted as T-X in which T means TiO_2 and X is calcining temperature. The phosphate-modified T is defined as PT-X-Y, in which Y is the concentration of phosphoric acid solution used.

2.2. Characterization of materials

The samples are tested by X-ray powder diffraction (XRD) with a Rigaku D/MAX-rA powder diffractometer, using Cu Kα radiation. Electron micrographs are taken on a JEOL JEM-2010 transmission electron microscope (TEM) operated at 200 kV. The specific surface areas of the samples are measured by a Brunauer–Emmett–Teller (BET) instrument (Micromeritics automatic surface area analyzer Gemini 2360, Shimadzu), with nitrogen adsorption at 77 K. The surface composition and elemental chemical state of the samples are examined by X-ray Photoelectron Spectroscopy (XPS) using a Kratos-AXIS ULTRA DLD apparatus with an Al(Mono) X-ray source, and the binding energies are calibrated with respect to the signal for adventitious carbon. The UV–vis diffuse reflectance (DRS) spectra are measured with a Shimadzu UV-2550 spectrometer.

Time-resolved surface photovoltage (TR-SPV) measurement is performed with a self-assembled device in air atmosphere, in which the sample chamber is connected to an ITO glass as the top electrode and to a steel substrate as the bottom electrode, and a 10 mm thick mica spacer is placed between the ITO glass and the sample to decrease the space charge region at the ITO-sample interface. The samples are excited by a 355 nm-laser radiation with 10 ns pulse width from a second harmonic Nd:YAG laser (Lab-130-10H, Newport, Co.). The laser intensity is modulated with an optical neutral filter and measured by a high-energy pyroelectric sensor (PE50BF-DIF-C, Ophir Photonics Group). The surface photovoltage spectroscopy (SPS) measurements of the samples are carried out with a home-built apparatus. The powder sample is sandwiched between two ITO glass electrodes, which are arranged in an atmosphere-controlled sealed container. The SPS signals are the potential barrier change of testing electrode surface between the presence of light and darkness.

Temperature-programmed desorption (TPD) of oxygen is conducted in a flow apparatus built by us. 30 mg of the powder sample is pretreated at 350 °C for 0.5 h in an ultrahigh-purity He flow, and then the sample is activated at 350 °C for 0.5 h in an ultrahigh-purity O_2 flow. After that, the sample sequentially adsorbs O_2 for 2 h at 25 °C. Finally, the desorbed O_2 amount is monitored by a gas chromatograph (GC-2014, Shimadzu) with a TCD detector.

2.3. Analysis of hydroxyl radical

0.04 g of TiO_2 powder is dispersed in 120 mL of 1×10^{-3} M coumarin aqueous solution in a quartz reactor. At given irradiation time, a certain amount of the solution is transferred into a Pyrex glass cell for the fluorescence measurement of 7-hydroxycoumarin at around 456 nm under the light excitation of 332 nm with a spectrofluorometer (PerkinElmer LS 55).

2.4. Photocatalytic experiment

The activities of the samples are evaluated by photodegradation of gas-phase acetaldehyde and liquid-phase phenol under 150 W Xenon lamp. 0.1 g of TiO_2 sample is placed in a mixed gas system containing 810 ppm of acetaldehyde, 20% of O_2, and 80% of N_2 to carry out photodegradation reactions for 1 h. The determination of acetaldehyde concentration is performed with a gas chromatograph (GC-2014, Shimadzu) equipped with a flame ionization detector. For photodegradation of phenol, 0.05 g of TiO_2 sample is dispersed in 80 mL of 15 mg/L phenol solution, and the irradiation lasts for 1 h. The phenol concentration is measured by the 4-aminoantipyrine spectrophotometric method at the characteristic optical absorption (510 nm) of phenol with a Shimadzu UV-2550 spectrophotometer after centrifugation.

3. Results and discussion

3.1. Structural characterization and surface composition

Fig. 1 and Table 1 show the XRD patterns and TEM images of unmodified and phosphate-modified TiO_2, and their corresponding XRD data and BET surface areas, respectively. It can be seen that the as-synthesized unmodified TiO_2 dried at 100 °C (T-100) is pure anatase TiO_2 with low crystallinity, small crystallite size of about 12 nm and large surface areas of about 72 $m^2\,g^{-1}$. According to its anatase (0 0 4) and (2 0 0) XRD diffraction peaks and the thickness and the side length of the nanosheet by the TEM image, it is confirmed that the T-100 grows along the [0 0 1] direction [3,12], and the percentage of highly reactive (0 0 1) facet is estimated to be approximately 71%. As the thermal treatment temperature increases, the intensities of (1 0 1) and (0 0 4) diffraction peaks are increased gradually, accompanied by the decreased full width at half-maximum (FWHM). Noticeably, the intensity of (2 0 0) one is reduced and its FWHM becomes large in Fig. 1 and in Fig. S1A. It means that the thickness of the nanosheet in the [0 0 1] direction is increased and its side length in the [1 0 0] direction becomes small, leading to the decreased percentage of the exposed (0 0 1) facet. It is calculated that the percentage of the exposed (0 0 1) facet is altered from 71 to 25% as the thermal treatment temperature is increased from 100 to 500 °C in Table 1. This is consistent with the observed results from TEM images in Fig. 1.

As expected, the modification with phosphoric acid is favorable to keep the (0 0 1) facet exposure percentage, even unchanged after thermal treatment at 500 °C, and still with 67% 0 0 1 facet at 650 °C corresponding to 14 nm crystallite size and 60.9 $m^2\,g^{-1}$ surface area (Fig. 1, Table 1 and Fig. S1B). And, it is shown (Fig. S1C) that the large amount of modified phosphoric acid is much obvious to retain high-percentage (0 0 1) facet exposure. It is found from F 1s XPS spectra (Fig. 2) that there is a certain amount (6.0%) of F for the T-100, which mainly results from the surface fluoride based on its XPS peak position at 684.5 eV, other than from the doped fluoride into the crystal

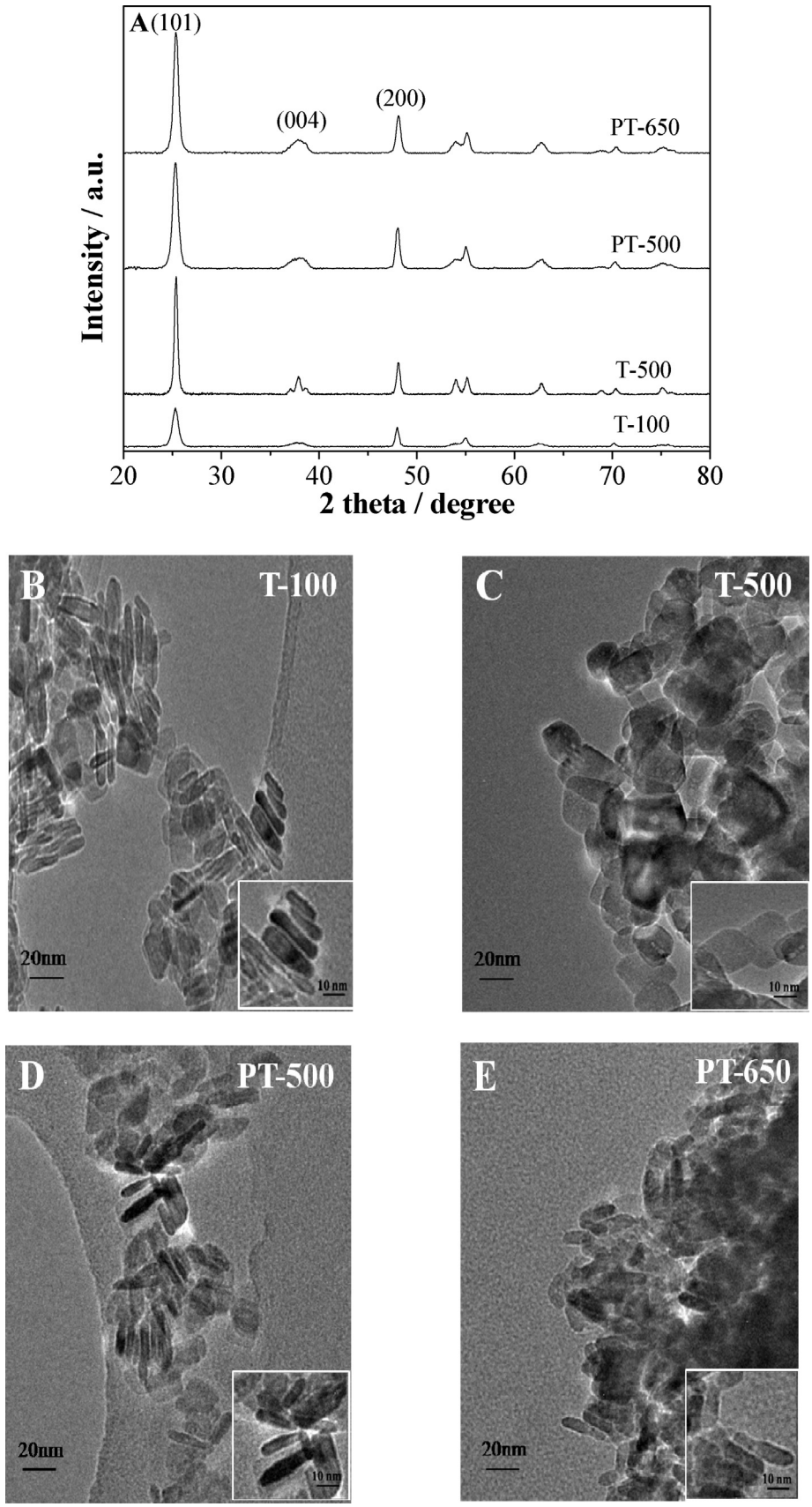

Fig. 1. XRD patterns and TEM images of T-100, T-500, PT-500 and PT-650 TiO_2. T-100 and T-500 mean the resulting TiO_2 treated at 100 and 500 °C, respectively, PT-500 and PT-650 are the phosphate modified TiO_2 treated at 500 and 650 °C, the same elsewhere unless mentioned.

Table 1
XRD data and BET surface areas of T-100, T-500, PT-500 and PT-650 TiO_2 samples.

Sample	[0 0 1] directions crystallite size (nm)	[1 0 0] directions crystallite size (nm)	Exposed {0 0 1} facets (%)	Crystallite size (nm)	Tested surface area (m^2g^{-1})
T-100	4.0	23.1	71	12	72.8
T-500	19.9	25.4	25	21	49.8
PT-500	4.2	23.5	70	12	70.6
PT-650	4.8	24.1	67	14	60.9

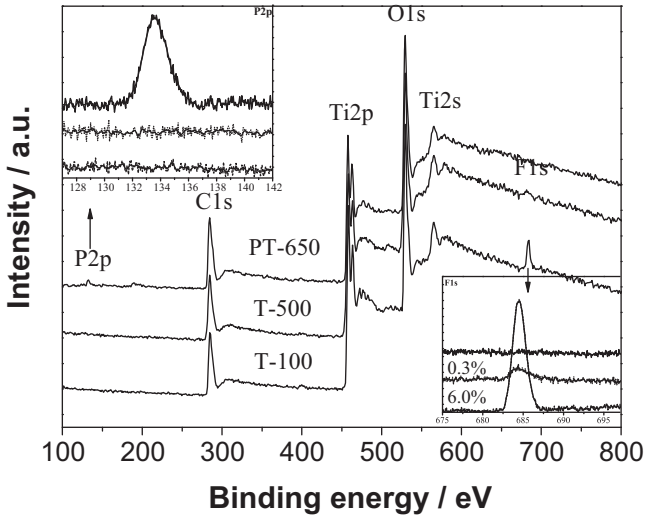

Fig. 2. XPS spectra of T-100, T-500 and PT-650 TiO_2 samples. The number for F XPS indicates the atomic concentration of residual F in TiO_2.

lattice [13]. After thermal treatment at 500 °C, the amount of surface residual fluoride of resulting TiO_2 (T-500) drastically decreases to 0.3%. This is responsible for the quick disappearance of the high-energy 0 0 1 facet. For the phosphoric acid-modified TiO_2 treated at 650 °C (PT-650), it is noticed that there is no residual F tested, and the P still exists as the chemical form of $[PO_4]^{3-}$ by the binding energy (133.6 eV) of P, linked to TiO_2 via the bidentate forms [14]. It implies that the modified phosphate groups would be firmly fixed on the surfaces of TiO_2 by substituting fluoride, leading to the enhanced thermal stability of 0 0 1-facet exposure.

3.2. Photoinduced charge separation

The properties of photogenerated charge carriers are mainly investigated by the time-resolved surface photovoltage (TR-SPV) measurements (Fig. 3A) and the surface photovoltage spectra (SPS, Fig. 3B). Widely accepted, when the electron-hole pairs are generated, they would be immediately separated under the built-in electric field, leading to the fast SPV component ($<10^{-5}$ s) [15]. For nano-sized *n*-type TiO_2, its built-in electric field would contribute to a weak, fast, positive SPV response [16]. And also, the photogenerated charge separation is influenced by the carrier diffusion process, corresponding to the slow SPV response ($>10^{-4}$ s) [17]. Since O_2 is favorable for capturing photogenerated electrons, it is acceptable that nano-sized TiO_2 should display a positive TR-SPV response via the carrier diffusion process and/or the built-in electric field [18]. It is seen that, compared to the T-100, the T-500 exhibits a low and short-lifetime TR-SPV response, while the PT-500 is high and long-lifetime one. In particular, the PT-650 displays further improved and lifetime-prolonged TR-SPV response. Consistent with the TR-SPV results, it demonstrates that the unmodified and H_3PO_4-modified TiO_2 treated at high temperature display much lower and higher SPS responses than T-100, respectively. For those samples, the SPS response is increased as the O_2 content becomes large (Fig. S2), indicating that the SPS attribute is

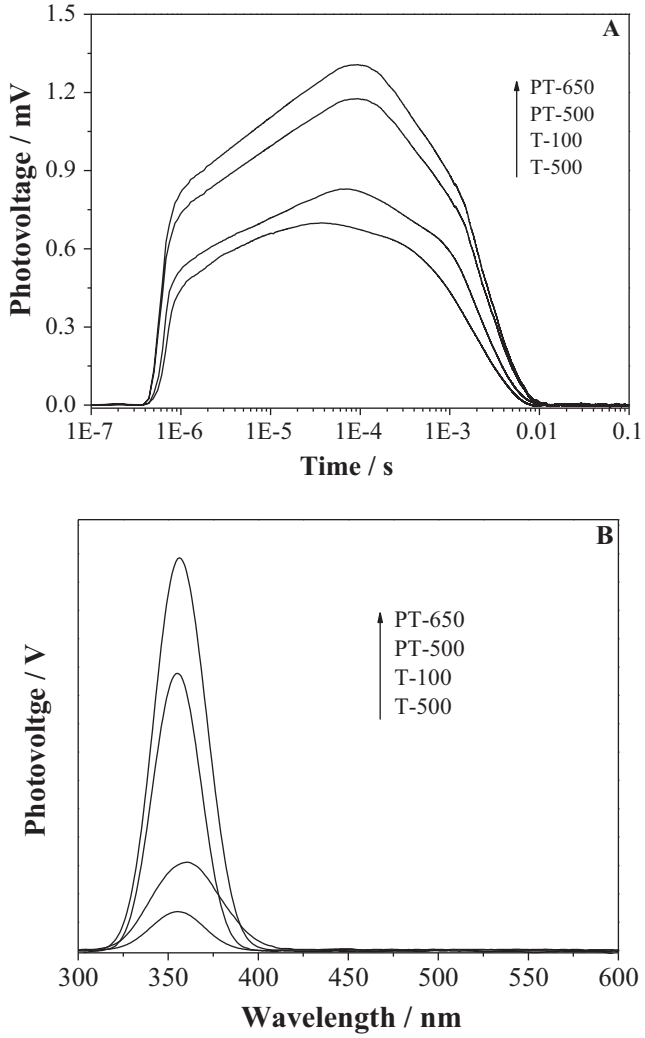

Fig. 3. TR-SPV (A) and SPS (B) responses of T-100, T-500, PT-500 and PT-650 TiO_2 samples. A 355 nm-laser radiation with 10 ns pulse width and a 500 W Xenon lamp are used for the TR-SPV and SPS measurements, respectively.

the same, depending on the adsorbed O_2 capturing photogenerated electrons [19]. In addition, it is demonstrated from Fig. S3 that the modification with a proper amount of H_3PO_4 would be beneficial for the SPS increase [20].

The strong and long-lifetime SPV response would correspond to the increased separation of photogenerated charges, which is further supported by the measurements of formed hydroxyl radical amounts on different TiO_2 after irradiation through the wide-used coumarin fluorescent method as a highly sensitive technique to detect the •OH amount [21]. As shown in Fig. 4 for four TiO_2 samples, the •OH amount gradually becomes large with increasing irradiation time. Compared with T-100, T-500 exhibits small amount, while PT-500 and PT-650 do large ones, and the PT-650 produces the largest amount of •OH among those samples. This is in good agreement with the TR-SPV and SPS results.

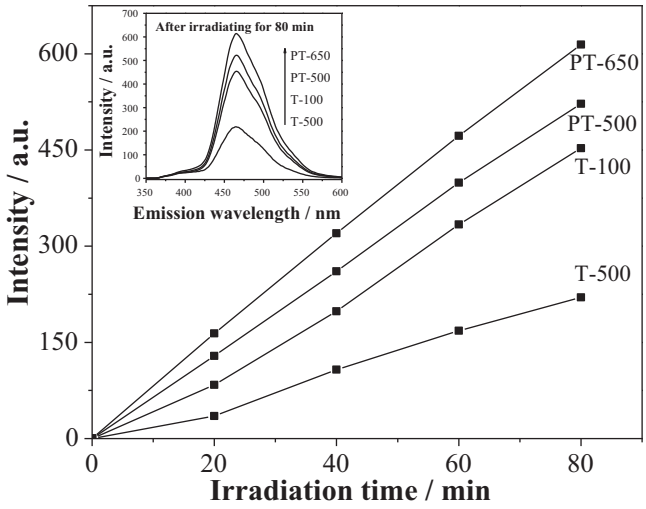

Fig. 4. Temporal profiles of hydroxyl radicals on T-100, T-500, PT-500 and PT-650 samples. Inset shows the fluorescence spectra related to the formed hydroxyl radical amount after irradiation for 80 min.

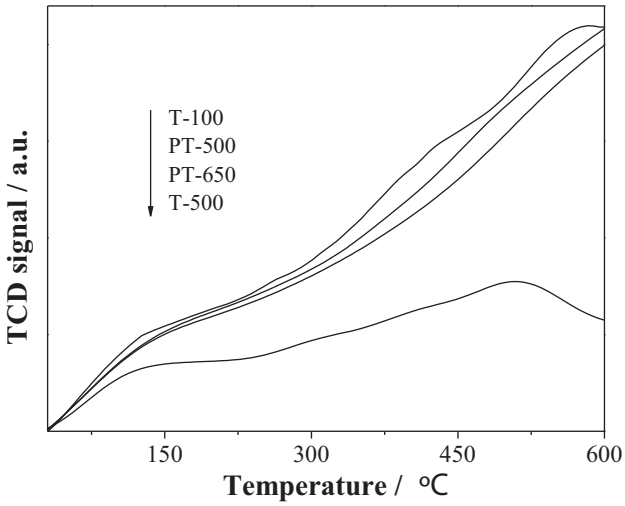

Fig. 6. Curves of O_2 temperature-programmed desorption of T-100, T-500, PT-500 and PT-650 TiO_2 samples.

3.3. Photocatalytic activities

Gas-phase acetaldehyde and liquid-phase phenol are chosen as model pollutants to evaluate photocatalytic activities of as-obtained TiO_2. The direct photolysis of the two pollutants mentioned above is neglectable compared with the photocatalytic degradation on TiO_2. The photodegradation rate is equal to the difference between the total degradation rate under illumination and the adsorption degradation rate without light, as shown in Fig. 5. One can see that there is an excellent linear relationship between $\ln(C/C_0)$ (C and C_0 are concentrations of acetaldehyde after and before light irradiation, respectively) and irradiation time, indicating that the photocatalytic degradation of acetaldehyde follows a pseudo-first-order kinetic reaction. As expected, PT-500 and PT-650 possess much higher photocatalytic activities for degrading gas-phase acetaldehyde and liquid-phase phenol than T-100, especially for PT-650 with superior photocatalytic performance to the internationally commercial P25 TiO_2 (Fig. S4). One can note that the rate constant of PT-650 (0.036 min^{-1} for photocatalytic degradation of acetaldehyde) is larger by about two times than that of the T-100, and the modification with a proper amount of phosphate groups corresponds to the high photoactivity (Fig. S5). If the used phosphate amount is too much, the photoactivity begins to decrease. In addition, the T-500 exhibits low photoactivity. Thus, it is concluded that the high photogenerated charge separation is responsible for the high photocatalytic activity.

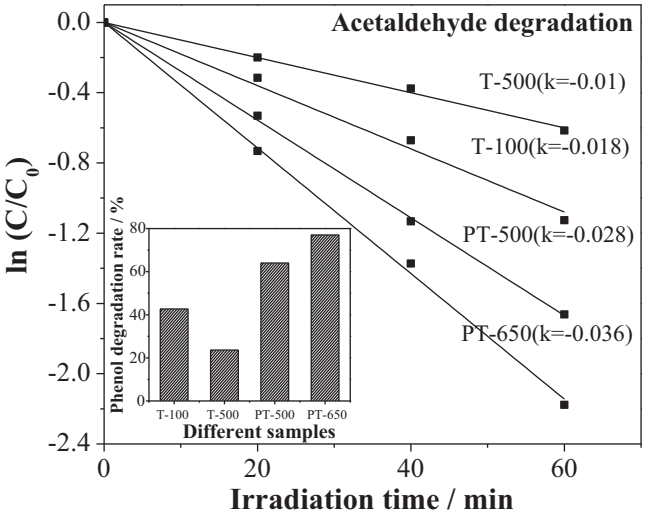

Fig. 5. Photocatalytic degradation rates of gas-phase acetaldehyde and liquid-phase phenol (inset) on different TiO_2 samples.

3.4. Discussion

Why could PT-500 and PT-650 display long-lived photogenerated charge carriers with high separation so as to improve its photocatalytic activity? It is mainly attributed to the following three points. Firstly, it still keeps a high-percentage (0 0 1) facet exposure. Since the (0 0 1) facets could provide oxidative sites while the (1 0 1) facets do reductive ones, the obtained sheet-like nanoparticles would facilitate an effective separation of photogenerated electron-hole pairs [22]. Secondly, it possesses high anatase crystallinity. In general, the high crystallinity makes electronic band perfect so as to enhance the built-in field strength, promoting charge separation, and the surface defect is decreased simultaneously, favorable for charge transportation [23,24]. Lastly, it could still remain large surface area, which is favorable for adsorption of reactants, like O_2. In the photocatalytic degradation of pollutants, the adsorption of O_2 is crucial for efficient photocatalysis since the adsorbed O_2 would be used to capture photogenerated electrons as a half-reaction [11,25]. It is demonstrated that the large surface area corresponds to the high amount of desorbed O_2 based on the O_2 temperature-programmed desorption measurements (Fig. 6), and PT-500 and PT-650 display slightly small amount of O_2 desorption compared with T-100. For T-500, its exposed (0 0 1) facet percentage and adsorbed O_2 amount are greatly decreased, leading to the weak separation of photogenerated charges.

4. Conclusions

In conclusion, the thermal stability of 0 0 1-facet-exposed nanocrystalline anatase TiO_2 is greatly enhanced by phosphate modification, and the modified TiO_2 treated at high temperature exhibits obviously lifetime-prolonged and separation-enhanced features of photogenerated charge carriers, which are mainly attributed to the synergetic effects of high-percentage 0 0 1-facet exposure, high anatase crystallinity, and strong ability to adsorb O_2. This, interestingly, leads to remarkably high photocatalytic activity for degrading gas-phase acetaldehyde and liquid-phase phenol,

compared to T-100. This work would provide with a feasible route to enhance thermal stability of exposed high-energy facet of nano-sized oxides, for highly desired activity as photocatalysts.

Acknowledgements

We are grateful for financial support from NSFC (21071048), the Program for Innovative Research Team in Chinese Universities (IRT1237), the Specialized Research Fund for the Doctoral Program of Higher Education (20122301110002) and the Chang Jiang Scholar Candidate Program for Heilongjiang Universities (2012CJHB003).

Appendix A. Supplementary data

Supplementary data associated with this article can be found, in the online version, at http://dx.doi.org/10.1016/j.apcatb.2013.08.029.

References

[1] X.Q. Gong, A. Selloni, J. Phys. Chem. B 109 (2005) 19560–19562.
[2] G. Liu, J.C. Yu, G.Q. Lu, H.M. Cheng, Chem. Commun. 47 (2011) 6763–6783.
[3] H.G. Yang, C.H. Sun, S.Z. Qiao, J. Zou, G. Liu, S.C. Smith, H.M. Cheng, G.Q. Lu, Nature 453 (2008) 638–641.
[4] D. Zhang, G. Li, X. Yang, J.C. Yu, Chem. Commun. 29 (2009) 4381–4383.
[5] H. Zhang, Y. Wang, P. Liu, Y. Han, X. Yao, J. Zou, H. Cheng, H. Zhao, ACS Appl. Mater. Interfaces 3 (2011) 2472–2478.
[6] Z. Wang, K. Lv, G. Wang, K. Deng, D. Tang, Appl. Catal. B Environ. 100 (2010) 378–385.
[7] D. Zhang, G. Li, H. Wang, K.M. Chan, J.C. Yu, Cryst. Growth Des. 10 (2010) 1130–1137.
[8] Y. Luan, L. Jing, Y. Xie, X. Sun, Y. Feng, H. Fu, ACS Catal. 3 (2013) 1378–1385.
[9] K. Lv, Q. Xiang, J. Yu, Appl. Catal. B Environ. 104 (2011) 275–281.
[10] X. Qin, L. Jing, G. Tian, Y. Qu, Y. Feng, J. Hazard. Mater. 172 (2009) 1168–1174.
[11] L. Jing, Y. Cao, H. Cui, J.R. Durrant, J. Tang, D. Liu, H. Fu, Chem. Commun. 48 (2012) 10775–10777.
[12] X.H. Yang, Z. Li, C. Sun, H.G. Yang, C. Li, Chem. Mater. 23 (2011) 3486–3494.
[13] J.C. Yu, J. Yu, W. Ho, Z. Jiang, L. Zhang, Chem. Mater. 14 (2002) 3808–3816.
[14] L. Kőrösi, S. Papp, I. Bertóti, I. Dékány, Chem. Mater. 19 (2007) 4811–4819.
[15] Y. Lin, D. Wang, Q. Zhao, M. Yang, Q. Zhang, J. Phys. Chem. B 108 (2004) 3202–3206.
[16] L. Jing, X. Sun, J. Shang, W. Cai, Z. Xu, Y. Du, H. Fu, Sol. Energy Mater. Sol. Cells 79 (2003) 133–151.
[17] X. Wei, T. Xie, L. Peng, W. Fu, J. Chen, Q. Gao, G. Hong, D. Wang, J. Phys. Chem. C 115 (2011) 8637–8642.
[18] L. Jing, X. Qin, Y. Luan, Y. Qu, M. Xie, Appl. Surf. Sci. 258 (2012) 3340–3349.
[19] Y. Luan, L. Jing, Q. Meng, H. Nan, P. Luan, M. Xie, Y. Feng, J. Phys. Chem. C 116 (2012) 17094–17100.
[20] Y. Cao, L. Jing, X. Shi, Y. Luan, J.R. Durrant, J. Tang, H. Fu, Phys. Chem. Chem. Phys. 14 (2012) 8530–8536.
[21] J. Yu, L. Qi, M. Jaroniec, J. Phys. Chem. C 114 (2010) 13118–13125.
[22] Z. Zheng, B. Huang, J. Lu, X. Qin, X. Zhang, Y. Dai, Chemistry 17 (2011) 15032–15038.
[23] G. Tian, H. Fu, L. Jing, B. Xin, K. Pan, J. Phys. Chem. C 112 (2008) 3083–3089.
[24] Y. Luan, L. Jing, M. Xie, X. Shi, X. Fan, Y. Cao, Y. Feng, Phys. Chem. Chem. Phys. 14 (2012) 1352–1359.
[25] W. Sun, Q. Meng, L. Jing, D. Liu, Y. Cao, J. Phys. Chem. C 117 (2013) 1358–1365.